A Bubbling Fluidization Model Using Kinetic Theory of Rough Spheres

Wang Shuai, Hao Zhenhua, Lu Huilin, Liu Goudong, Wang Jiaxing, and Xu Pengfei
School of Energy Science and Engineering, Harbin Institute of Technology, Harbin 150001, China

DOI 10.1002/aic.12590
Published online March 31, 2011 in Wiley Online Library (wileyonlinelibrary.com).

Collisional motion of inelastic rough spheres is analyzed on the basis of the kinetic theory for flow of dense, slightly inelastic, slightly rough sphere with the consideration of gas–solid interactions. The fluctuation kinetic energy of particles is introduced to characterize the random motion of particles as a measure of the translational and rotational velocities fluctuations. The kinetic energy transport equation is proposed with the consideration of the redistribution of particle kinetic energy between the rotational and translational modes and kinetic energy dissipation by collisions. The solid pressure and viscosity are obtained in terms of the particle roughness and restitution coefficient. The partition of the random-motion kinetic energy of inelastic rough particles between rotational and translational modes is shown to be strongly affected by the particle restitution coefficient and roughness. Hydrodynamics of gas–solid bubbling fluidized beds are numerically simulated on the basis of the kinetic theory for flow of rough spheres. Computed profiles of particles are in agreement with the experimental measurements in a bubbling fluidized bed. The effect of roughness on the distribution of energy dissipation, kinetic energy, and viscosity of particles is analyzed. © 2011 American Institute of Chemical Engineers *AIChE J,* 58: 440–455, 2012
Keywords: computational fluid dynamics, fluid mechanics, fluidization, hydrodynamics, kinetic theory of granular flow, collisions of rough spheres

Introduction

Gas–solid fluidized beds operating in the bubbling regime have been widely used in various fields of chemical engineering and of the power industry due to the highest contact efficiency between the phases, which leads to a higher conversion and a better heat distribution. Therefore, the prediction of fluidized bed dynamics has been an active area of research. The numerical modeling of bubbling fluidized beds presents particular difficulties due to the complex involved in the system related to the particle–particle interactions.[1] The Eulerian–Eulerian two-phase approach is used to simulate flow behavior in fluidized beds in the combination with the kinetic theory of granular flow (KTGF). The KTGF model is based on the analogy between particles and the molecules of dense gases.[2] The solid-phase stress results from both translational motion and direct collisions of particles on the basis of Grad's theory[3] or a linear theory developed by Jenkins and Richman.[4] These results were valid for granular flows without an interstitial gas. Gidaspow[5] generalized the KTGF to gas-particle flows. An important difference is that collisions between molecules in the dense gas are considered as elastic, whereas the particle collisions are inelastic causing kinetic energy dissipating into heat. In the original KTGF, particles are assumed to be slightly inelastic and smooth spheres, and fluctuation energy dissipation only comes from binary inelastic collisions. The approach uses a one-equation model to describe the turbulent kinetic energy of the particle, introduced with the concept of granular temperature of particles, considering both dilute and dense cases.

Correspondence concerning this article should be addressed to L. Huilin at huilin@hit.edu.cn.

Many research groups have been involved in numerical simulations of hydrodynamics in fluidized beds with kinetic granular theory, and encouraging results have been reported in literature.[6-23] The most significant application of KTGF to fluidization is reviewed by Arastoopour[24] and Gidaspow et al.[25] in the Flour-Daniel *AIChE* lecture.

The original KTGF models of Savage and Jeffrey,[26] Lun et al.,[27] and Jenkins and Richman[4] as well as the generalized model of Gidaspow[5] are derived for nearly elastic particles ($1.0 - e$ must be small, where e is the coefficient of restitution) in translational motion. In realistic situation, particle surface cannot be perfectly smooth and particles are frictional as well as inelastic. During a collision of rough particles, the fluctuation energy is dissipated from inelasticity and frictions of particles. The frictional particle collision also results in the particle rotation which gives additional loss of the energy. As a result, particles can rotate with angular velocity ω under rapid rates of deformation. Jenkins and Mancini[28] and Lun and Savage[29] studies were the first comprehensive investigations that consider rough, inelastic spherical particles. In the kinetic theory for flow of identical, slightly frictional, inelastic spheres proposed by Lun[30] and Jenkins and Zhang,[31] two granular temperatures are involved. The first is the translational granular temperature θ_t, which measures the energy associated with the translational velocity fluctuations, defined as $\theta_t = \langle C^2 \rangle /3$, where C is the fluctuating velocity of particles. The second is the rotational granular temperature θ_r, which measures the energy associated with the angular velocity fluctuations, defined as $\theta_r = (1/3m)\langle I\varpi^2 \rangle$, where I is the moment of inertia, ϖ is the angular velocity fluctuation, and m is the mass of a particle. Collisional motion of rough inelastic spheres was analyzed on the basis of the kinetic Boltzmann-Enskog equation.[32] The Chapman-Enskog method for gas kinetic theory is modified to derive the Euler-like hydrodynamic equations, possessing constant roughness and inelasticity. Sun and Battaglia[33] implemented a model from kinetic theory for rapid flow of identical, slightly frictional, nearly elastic spheres[31] into the MFIX CFD code.[34] In this model, the conservation of rotational granular energy is approximately satisfied by requiring that the net rate of energy production for the angular velocity fluctuations is zero. The influence of friction on the collisional transfer of momentum and translational energy is negligible. Only the dissipation rates for translational and rotational granular energy are influenced by friction. They found that the model captures the bubble dynamics and time-averaged bed behavior. Shuyan et al.[35] simulated flow behavior of particles in the bubbling fluidized bed based on the kinetic theory for flow of dense, slightly inelastic, slightly rough sphere proposed by Lun[30] to account for rough sphere binary collisions and the frictional stress model proposed by Johnson et al.[36] to consider the frictional contact forces between particles. By setting the rotational energy dissipation rate to zero in a steady, homogeneous shear flow, the ratio of the rotational granular temperature to the translational granular temperature is correlated with the roughness coefficient of particles. Thus, the kinetic theory for slightly frictional, nearly elastic spheres is used to simulate flow behavior of clusters in the riser.[37] Simulated results show that particle rotations reduce the cluster size and alter the particle flows and distributions through more particle fluctuation energy dissipations.

In present work, a two-fluid model with the kinetic theory for flow of dense, slightly inelastic, slightly rough sphere proposed by Goldshtein and Shapiro[32] is used to study the flow behavior of gas and particles in a bubbling fluidized bed. The particle average fluctuation kinetic energy is introduced to govern the mechanism dominating kinetic energy transformation in flow of particles. The conservation equation of fluctuating kinetic energy is proposed to take the transfer of particle kinetic energy between the rotational and translational degrees of freedom and also the energy losses into account. The model of fluctuating kinetic energy of particles is incorporated into the two-fluid model. Distributions of concentrations and velocities of gas and particles are predicted in the bubbling fluidized bed. Computed results are compared with solids concentration and bed expansion ratios measured by Taghipour et al.[38]

Kinetic Theory for Granular Flow of Rough Sphere

Governing equations

The kinetic theory is aimed at deriving the appropriate hydrodynamic equations governing granular flows.[5] These equations may be obtained on the basis of an appropriately modified Boltzmann equation either by approximate methods of gas kinetic theory[4,27] or by a rigorous application of a variant of the Champan-Enskog solution scheme.[2] The latter method has the advantage of yielding the right form of the hydrodynamic equations and, simultaneously, establishing their validity range. Considering an ensemble of identical rough spherical particles with spherically symmetric mass distribution, the chaotic translational and rotational motions are assumed in an effectively infinite spatial domain. In a collision between frictional spheres, the collisional impulse has a tangential component and a normal component. The change in the normal velocity is determined by the normal restitution coefficient e, which can range from 0.0 to 1.0. An e value of 0.0 indicates a complete loss of normal velocity, whereas an e value of 1.0 indicates no loss of normal velocity. Changes in spin and in the tangential velocity depend on the frictional properties of the surfaces. The frictional properties of the surface are characterized by the roughness β (tangential restitution coefficient).[30,31] A constant roughness β was used to characterize the ratio of the tangential component of the relative velocity of the point of contact after a collision to its value before a collision. The value of this constant coefficient β is assumed to be between -1.0 and $+1.0$. When β equals -1.0, the spheres are frictionless and there is no change in the tangential component of the relative velocities. Increasing value of β represents the increasing degrees of particle surface friction. When β equals $+1.0$, the tangential component of this velocity reverses completely and the spheres are said to be perfectly rough. In fact, β is a mixed approximate expression for both friction $-1.0 < \beta < 0$ and tangential restitution $0 < \beta < +1.0$.

For simplification, the following assumptions are made: (1) Particles have a uniform size with the same density. (2) Statistical expectation values of the particle ensemble may be expressed via the singlet distribution function $f_1 = f(\mathbf{x}, \Omega, t)$ where the variable Ω represents translational and angular

velocities of particles (c and ω). The pair correlations of each two particles is expressed via the pair distribution function $f^{(2)} = f(\mathbf{x}_1, \Omega_1, \mathbf{x}_2, \Omega_2, t)$. (3) The probabilities of triple and multiple collisions are negligible. Based on the above assumptions and using the technique used in the classical kinetic theory,[2] the Boltzmann equation for the singlet distribution function f with rotation is as follows[5,30-32]:

$$\frac{\partial f}{\partial t} + c \cdot \frac{\partial f}{\partial x} + F \cdot \frac{\partial f}{\partial c} = \frac{\sigma}{4} \iiint [f^{(2)}(x, \Omega_1, x + dk, \Omega_2, t) - f^{(2)}(x, \Omega_1, x - dk, \Omega_2, t)] \sigma^2 (c_{21} \cdot k) d^6\Omega_1 d^6\Omega_2 d^2k \quad (1)$$

where c is the instantaneous velocity of particles. σ is the diameter of a particle. F is the external force per unit of mass acting on a sphere. $d^6\Omega_i = d^3c_i d^3\omega_i$ ($i = 1, 2$). The right term in Eq. 1 is the rate of change of the distribution function due to particle collisions. Multiplying Eq. 1 by a function $\phi(\Omega)$ and integrating over the whole velocity domain gives a transport equation, as proposed by Chapman and Cowling.[2] The transport equation for the mean quantity, $\langle \phi \rangle$, is

$$\frac{D}{Dt}(n\langle\phi\rangle) + \frac{\partial}{\partial \mathbf{x}} \cdot (n\langle \mathbf{C}\phi \rangle) + \langle n\phi \rangle \frac{\partial}{\partial \mathbf{x}} \cdot \mathbf{u} + n \frac{D\mathbf{u}}{Dt} \cdot \left\langle \frac{\partial \phi}{\partial \mathbf{C}} \right\rangle - n \left\langle \mathbf{F} \cdot \frac{\partial \phi}{\partial \mathbf{C}} \right\rangle + n \left\langle \mathbf{C} \frac{\partial \phi}{\partial \mathbf{C}} \right\rangle : \frac{\partial \mathbf{u}}{\partial \mathbf{x}} = \mathrm{Coll}(\phi) \quad (2)$$

where C is the fluctuation velocity, $\mathbf{C} = u - \mathbf{c}$, u is the mean velocity of particles. The collisional rate of change of ϕ per unit volume, Coll (ϕ), is the integral, over all possible binary collisions, of the change of ϕ due to a binary collision multiplied by the probability of such a collision[5,30,32]

$$\mathrm{Coll}(\phi) = \chi(\phi) - \frac{\partial}{\partial x_i} \psi(\phi) \quad (3)$$

$$\chi(\phi) = \frac{1}{2} \iiint \sigma^2 (k \cdot c_{21}) [(\phi_1' - \phi_1) + (\phi_2' - \phi_2)] f^{(2)} \times (\mathbf{x} + \sigma\ \mathrm{k}, c_1, \omega_1; x, c_2, \omega_2, t) dk dc_1 dc_2 d\omega_1 d\omega_2 \quad (3a)$$

$$\psi(\phi) = -\frac{\sigma}{4} \iiint \sigma^2 (k \cdot c_{21}) [(\phi_1' - \phi_1) - (\phi_2' - \phi_2)] f^{(2)} \times (\mathbf{x} + \sigma\ \mathrm{k}, c_1, \omega_1; x, c_2, \omega_2, t) dk dc_1 dc_2 d\omega_1 d\omega_2 \quad (3b)$$

where $\chi(\phi)$ and $\psi(\phi)$ can be identified as the volumetric source term and the collisional transfer flux vector, respectively. Formula (3a) describes the collisional rate of change of ϕ. For the model investigated here, this expression takes the transfer of particle kinetic energy between their rotational and translational degrees of freedom into account.

By taking ϕ in Eq. 3 to be the velocity, the relationship between the pre- and post-collisional velocities can be shown to be

$$c_1' - c_1 = -\eta_2 c_{12} - (\eta_1 - \eta_2) k (k \cdot c_{12}) + \frac{1}{2} \eta_2 \sigma k \times (\omega_1 + \omega_2) \quad (4)$$

$$c_2' - c_2 = \eta_2 c_{12} + (\eta_1 - \eta_2) k (k \cdot c_{12}) - \frac{1}{2} \eta_2 \sigma k \times (\omega_1 + \omega_2) \quad (5)$$

$$\omega_1' - \omega_1 = \omega_2' - \omega_2 = -\frac{2\eta_2}{\sigma K} (k \times c_{12}) + \frac{\eta_2}{K} (k \cdot (\omega_1 + \omega_2)) k - \frac{\eta_2}{K} (\omega_1 + \omega_2) \quad (6)$$

where the definition of coefficients η_1, η_2, and K are given in Table 1. The coefficient K is the nondimensional parameter of moment of inertia. Parameter K can very in value from zero when the mass is concentrated at the center of the sphere, to 2/3 when the mass is uniformly distributed over the surface of the sphere. For the case of uniform solid sphere treated here $K = 2/5$.

The collision of particles is accompanied by kinetic energy losses, associated with inelasticity of collisions and surface friction. The effect of these losses is to increase the particle internal energy. Therefore, a constant source of energy is needed to sustain the collisions of fluidized particles. The kinetic theory involves two measures of the strength of these fluctuations: the translational temperature and the rotational temperature. The kinetic energy of random motion of particles, E, consists of a translational kinetic energy part and a rotational kinetic part. The mean translational fluctuation kinetic energy is $m\langle C^2 \rangle/2 = 3m\theta_t/2$, where C is the fluctuating translational velocity of particles, and the mean rotational fluctuation kinetic energy is $I\langle \varpi^2 \rangle/2 = 3m\theta_r/2$, where $\langle\rangle$ represents the ensemble average. The fluctuating angular velocity of particles is $\varpi = \omega - \omega_0$, where ω_0 is the mean particle spin velocity. θ_t and θ_r are the translational granular temperature and rotational granular temperature, respectively. Thus, the particle fluctuation kinetic energy is[2,32]

$$e_o = \frac{E}{m} = \left\langle \frac{1}{3} C^2 + \frac{I\varpi^2}{3m} \right\rangle = (\theta_t + \theta_r) \quad (7)$$

In contrast to the definition of fluctuation kinetic energy by Goldshtain and Shapiro,[32] the kinetic energy in Eq. 7 includes the translational and rotational contributions.

In Eqs. 3a and 3b, they include the pair distribution function $f^{(2)}$. Here, we used a closing relation for the singlet distribution function by invoking the generally accepted assumption of molecular chaos by modifying to include the equilibrium radial distribution function at contact g_o:

$$f^{(2)}(\mathbf{x} + \sigma\ \mathbf{k}, c_1, \omega_1; x, c_2, \omega_2, t) = g_o f_1(\mathbf{x} + \sigma\ \mathbf{k}, c_1, \omega_1, t) f_2(x, c_2, \omega_2, t) \quad (8)$$

The radial distribution function is independent of particle collisional properties.[2] The first approximation for the singlet distribution function f at the steady-state with no collisions is the Maxwell Boltzmann distribution[2,32]

$$f(r, c, \omega; t) = \frac{nI^{3/2}}{\pi^3 (\alpha_t \alpha_r)^{3/2} e_o^3} \exp\left[-\frac{(c-u)^2}{\alpha_t e_o} - \frac{\omega^2 I}{m \alpha_r e_o} \right] \quad (9)$$

where n is the number density of particles. I is the moment of inertia. For uniform spheres, $I = 0.1m\sigma^2$. From Eq. 7, the kinetic energy e_o of particle random motion is expressed via granular kinetic translational θ_t and rotational θ_r temperatures[32]:

$$\theta_t = \frac{3}{4} \alpha_t e_o \quad \text{and} \quad \theta_r = \frac{3}{4} \alpha_r e_o \quad (10)$$

Table 1. Equations of Gas-Solid Flow in Fluidized Beds

(1) Continuity equations of gas and particles

$$\frac{\partial}{\partial t}(\varepsilon_g \rho_g) + \nabla \cdot (\varepsilon_g \rho_g \mathbf{u}_g) = 0 \tag{T1-1}$$

$$\frac{\partial}{\partial t}(\varepsilon_s \rho_s) + \nabla \cdot (\varepsilon_s \rho_s u_s) = 0 \tag{T1-2}$$

(2) Conservation of momentum of gas and solids

$$\frac{\partial}{\partial t}(\varepsilon_g \rho_g \mathbf{u}_g) + \nabla \cdot (\varepsilon_g \rho_g \mathbf{u}_g \mathbf{u}_g) = -\varepsilon_g \nabla p + \nabla \cdot \tau_g - \beta_{gs}(\mathbf{u}_g - \mathbf{u}_s) + \varepsilon_g \rho_g \mathbf{g} \tag{T1-3}$$

$$\frac{\partial}{\partial t}(\varepsilon_s \rho_s \mathbf{u}_s) + \nabla \cdot (\varepsilon_s \rho_s \mathbf{u}_s \mathbf{u}_s) = -\varepsilon_s \nabla p - \nabla \cdot (p_s I) + \nabla \tau_s + \beta_{gs}(\mathbf{u}_g - \mathbf{u}_s) + \varepsilon_s \rho_s \mathbf{g} \tag{T1-4}$$

(3) Kinetic energy equation of solids

$$\frac{3}{2}\left[\frac{\partial}{\partial t}(\varepsilon_s \rho_s e_o) + \nabla \cdot (\varepsilon_s \rho_s e_o \mathbf{u}_s)\right] = \nabla \cdot (\kappa_s \nabla e_o) + (\nabla p_s I + \tau_s) : \nabla \mathbf{u}_s - \gamma_s - D_{gs} - 3\beta_{gs} e_o \tag{T1-5}$$

(4) Constitutive relations

(a) Gas phase viscous stress tensor

$$\tau_g = \mu_g[\nabla \mathbf{u}_g + (\nabla \mathbf{u}_g)^T] - \frac{2}{3}\mu_g(\nabla \cdot \mathbf{u}_g)\mathbf{I} \tag{T1-6}$$

(b) Stress tensor of solids

$$\tau_s = \mu_s[\nabla \mathbf{u}_s + (\nabla \mathbf{u}_s)^T] + \xi_b(\nabla \cdot \mathbf{u}_s)I + \xi_s \delta_{ij} \times \nabla \times \mathbf{u}_s \tag{T1-7}$$

(c) Solid pressure

$$p_s = \frac{3}{4}\alpha_t \varepsilon_s \rho_s e_o + \frac{3}{2}\alpha_t \varepsilon_s^2 \rho_s g_o (1+e) e_o \tag{T1-8}$$

$$\alpha_t = \frac{2}{3a}[(a-b) + (a^2+b^2)^{1/2}] \tag{T1-9}$$

$$a = (1-\beta^2)\frac{1-K}{1+K} - 1 + e^2 \quad \text{and} \quad b = 2K\left(\frac{1+\beta}{1+e}\right)^2 \tag{T1-9a}$$

(d) Shear viscosity of solids

$$\mu_s = \frac{2}{5}\varepsilon_s g_o \sigma \rho_s \sqrt{\frac{e_o}{\pi}}(4\eta_1 + 3\eta_2)\left[\varepsilon_s \sqrt{\frac{3\alpha_t}{4}} - \sqrt{\frac{3}{128}}\pi \frac{\alpha_t \pi}{g_0}(a_{kt} + 2\varepsilon_s g_o (1+e) a_{ct})\right] + \mu_{dil}\left\{\frac{1 + \frac{8}{5}[\eta_1(3\eta_1 - 2) + 0.5\eta_2(6\eta_1 - 1 - 2\eta_2 - \frac{2\eta_2 \alpha_r}{K\alpha_t})]\varepsilon_s g_o}{g_o\left[(2-\eta_1-\eta_2)(\eta_1+\eta_2) + \frac{\eta_2^2 \alpha_r}{6K\alpha_t}\right]}\right\}\left\{1 + \frac{4}{5}[2\eta_1 + 3\eta_2]\varepsilon_s g_o\right\} \tag{T1-10}$$

$$\mu_{dil} = \frac{5\sigma\rho_s}{96}\sqrt{\frac{3\pi\alpha_t e_0}{4}} \tag{T1-11}$$

$$\alpha_r = \frac{2}{3a}[(a+b) - (a^2+b^2)^{1/2}] \tag{T1-12}$$

$$a = (1-\beta^2)\frac{1-K}{1+K} - 1 + e^2, \quad b = 2K\left(\frac{1+\beta}{1+e}\right)^2$$

$$\eta_1 = \frac{(1+e)}{2}, \ \eta_2 = \frac{(1+\beta)K}{2(1+K)}, \ K = \frac{4I_p}{m\sigma^2}, \ a_{kt} = -\frac{3}{4}\alpha_t \alpha_r \chi^{-1}$$

$$a_{ct} = a_{kt}\left\{1 - \frac{3}{2}(1-e) - \left(\frac{1-\beta^2}{1+K}\right)\left[\frac{K\alpha_t + \alpha_r}{\alpha_t(1+e)}\right]\right\} + \frac{4\eta_2\alpha_t}{(1+e)K}\left[\eta_2 + \left(\frac{\eta_2}{K} - 1\right)\frac{\alpha_r}{\alpha_t}\right]$$

$$\chi = \sqrt{\frac{\pi\alpha_t}{2}}\left\{\frac{3}{4}(1-e^2)\alpha_t(3\alpha_t - \alpha_r) + \frac{3}{4}\left(\frac{1-\beta^2}{1+K}\right)[(3K-3)\alpha_t\alpha_r + \alpha_r^2 - K\alpha_t^2] + \frac{4\eta_2}{K}\left[3\eta_2\alpha_t + \left(1 - \frac{\eta_2}{K}\right)(2\alpha_t - \alpha_r)\right]\right\}$$

(*Continued*)

(e) Bulk viscosity of solids

$$\xi_b = \frac{8}{3}\varepsilon_s g_o \sigma \rho_s \eta_1 \sqrt{\frac{e_o}{\pi}}\left[\varepsilon_s\sqrt{\frac{3\alpha_t}{4}} - \sqrt{\frac{3}{128}\pi}\frac{\alpha_t \pi}{g_0}(a_{kt} + 2\varepsilon_s g_o(1+e)a_{ct})\right] \tag{T1-13}$$

(f) Spin viscosity

$$\xi_s = \frac{192(1+\beta)K}{10\pi(1+K)}\mu_{dil}\varepsilon_s^2 g_o \tag{T1-14}$$

(g) Radial distribution function

$$g_o = \left[1 - \left(\frac{\varepsilon_s}{\varepsilon_{s,max}}\right)^{1/3}\right]^{-1} \tag{T1-15}$$

(h) Thermal conductivity coefficient of solids

$$k_s = \frac{3k_{dil}}{4g_0\Pi_1}[\alpha_t(\Pi_2+\Pi_4) + \alpha_r(\Pi_3+\Pi_5)] + \frac{9}{5}\varepsilon_s g_0 \frac{k_{dil}}{g_0\Pi_1}\left(\eta_1 + \frac{2}{3}\eta_2\right)[\alpha_t\Pi_2 + \alpha_r\Pi_3]$$
$$+ \frac{3\sqrt{3\alpha_t e_o}}{\sqrt{4\pi}}\alpha_t(\eta_1+\eta_2)\varepsilon_s^2\rho_s g_0\sigma + \frac{2\eta_2}{K}\frac{k_{dil}}{g_0\Pi_1}\varepsilon_s g_0[\alpha_t\Pi_4 + \alpha_r\Pi_5] + \frac{3\eta_2}{K}\varepsilon_s^2\rho_s g_0\sigma\alpha_r \tag{T1-16}$$

$$k_{dil} = \frac{5\sigma\rho_s}{15}\sqrt{\frac{3\pi\alpha_t e_0}{4}}\frac{(1+K)^2}{6+13K} \tag{T1-17}$$

$$\Pi_1 = \frac{1}{24}(3a_3a_8 - 25a_1a_6),\ \Pi_2 = \frac{1}{15}(6a_5a_8 + 10a_1a_7\varepsilon_s g_0),\ \Pi_3 = \frac{2}{15}(5a_1a_4 + 3a_2a_8\varepsilon_s g_0)$$
$$\Pi_4 = \frac{1}{25}(5a_5a_6 + a_3a_7\varepsilon_s g_0),\ \Pi_5 = \frac{1}{25}(a_3a_4 + 5a_2a_6\varepsilon_s g_0)$$
$$a_1 = \frac{\eta_2^2}{K},\ a_2 = 4a_1(2\eta_1 - 1),\ a_3 = 41(\eta_1+\eta_2) - 33(\eta_1+\eta_2)^2 + 50\eta_1\eta_2 - \frac{7a_1\alpha_r}{\alpha_t}$$
$$a_4 = \frac{3}{2} + \frac{a_2\varepsilon_s g_o}{K},\ a_5 = \frac{5}{2} + \left[4(6\eta_1^3 - \eta_2^3) - 2\eta_1(9\eta_1 + 4\eta_2) + 8a_1\eta_1\left(2K + \frac{\alpha_r}{\alpha_t}\right)\right]\varepsilon_s g_o$$
$$a_6 = a_1\left(3 + \frac{\alpha_r}{K\alpha_t}\right) - \frac{a_1\alpha_r}{\eta_2\alpha_t},\ a_7 = -16\eta_1 a_1 + a_2 + 8a_6\eta_1,\ a_8 = (\eta_1+\eta_2) + \frac{1}{3\eta_2}a_1(7 - 4\eta_1) - a_1\left(2 + \frac{1}{K}\right)$$

(i) Translational fluctuation energy dissipation rate

$$\gamma_s = -3\varepsilon_s^2\rho_s g_0\alpha_t e_o\frac{3\sqrt{3}}{2\sigma}\sqrt{\frac{\alpha_t e_o}{\pi}}\left[1 - e^2 + \left(\frac{1-\beta^2}{1+k}\right)\left(K + \frac{\alpha_r}{\alpha_t}\right)\right] + \frac{3\varepsilon_s\rho_s e_o}{4}[C_1\alpha_t + 2C_2\alpha_t\varepsilon_s g_o(1+e)]\nabla\cdot\boldsymbol{u}_s$$
$$C_1 = a_{kt}\lambda,\ C_2 = a_{ct}\lambda + \frac{3}{2}(1-e) + \left(\frac{1-\beta^2}{1+K}\right)\left[\frac{K\alpha_t + \alpha_r}{\alpha_t(1+e)}\right] \tag{T1-18}$$
$$\lambda = -\sqrt{\frac{\pi\alpha_t}{2}}\left[3(1-e^2) + \left(\frac{1-\beta^2}{1+K}\right)\left(3K - 2 + \frac{\alpha_r}{\alpha_t}\right)\right]$$

(j) Fluctuating energy exchange from gas and solids

$$D_{gs} = \frac{2}{(3\alpha_t)^{1.5}}\frac{\sigma\rho_s}{\sqrt{\pi e_o}g_o}\left(\frac{18\mu_g}{\sigma^2\rho_s}\right)^2|\mathbf{u}_g - \mathbf{u}_s|^2 \tag{T1-19}$$

(k) Interphase momentum exchange

$$\beta_{gs} = \varphi_{gs}\beta|_E + (1-\varphi_{gs})\beta|_W \tag{T1-20}$$

$$\beta|_E = 150\frac{\varepsilon_s^2\mu_g}{\varepsilon_g^2\sigma^2} + 1.75\frac{\rho_g\varepsilon_s}{\varepsilon_g\sigma}|\mathbf{u}_g - \mathbf{u}_s| \qquad \varepsilon_g \le 0.8 \tag{T1-21}$$

$$\beta|_W = \frac{3C_d\varepsilon_g\varepsilon_s\rho_g|\mathbf{u}_g - \mathbf{u}_s|}{4\sigma}\varepsilon_g^{-2.65} \qquad \varepsilon_g > 0.8 \tag{T1-22}$$

$$\varphi_{gs} = \frac{\arctan[150\times 1.75(0.2-\varepsilon_s)]}{\pi} + 0.5$$
$$C_d = \begin{cases}\frac{24}{Re}(1 + 0.15Re^{0.687}) & Re \le 1000\\ 0.44 & Re > 1000\end{cases} \tag{T1-23}$$
$$Re = \sigma\varepsilon_g\rho_g|\mathbf{u}_g - \mathbf{u}_s|/\mu_g$$

where the parameters α_t and α_r satisfy the following normalization condition[32]

$$\alpha_t + \alpha_r = \frac{4}{3} \tag{11}$$

assuring the proper behavior of the energy partition in the limiting cases $e = |\beta| = 1$.

Using Eq. 2 with ϕ being particle mass m, linear momentum (mu), and kinetic fluctuation energy (me_0), one can be obtained the conservation equations of mass, momentum, and kinetic fluctuation energy for solids phase. Table 1 lists the equations for flow of gas and solids phases used in present simulations. The balance equations of mass and momentum for solids phase are[5]

$$\frac{\partial}{\partial t}(\varepsilon_s \rho_s) + \nabla \cdot (\varepsilon_s \rho_s u_s) = 0 \tag{12}$$

$$\frac{\partial}{\partial t}(\varepsilon_s \rho_s u_s) + \nabla \cdot (\varepsilon_s \rho_s u_s u_s) = -\varepsilon_s \nabla p - \nabla p_s + \nabla \cdot \tau_s + \varepsilon_s \rho_s g + \beta(u_g - u_s) \tag{13}$$

where p_s is the solid pressure and τ_s the stress tensor of particles.

Using Eq. 2 with ϕ being kinetic energy of random motion e_o, one can be obtained the following conservation equation of solids fluctuating energy

$$\frac{3}{2}\left[\frac{\partial}{\partial t}(\varepsilon_s \rho_s e_o) + \nabla \cdot (\varepsilon_s \rho_s e_o u_s)\right] = \nabla \cdot (\kappa_t \nabla e_o) + (\nabla p_s I + \tau_s) : \nabla u_s - \gamma_s - D_{gs} - 3\beta_{gs} e_o \tag{14}$$

The two terms on the left-hand side of Eq. 14 represent the accumulation and convection of kinetic fluctuation energy, respectively. In the right-hand side of Eq. 14, the first-term describes the conductive transport of kinetic fluctuation energy. The second-term models the production of kinetic fluctuation energy due to irreversible deformation of the solid phase velocity field. The third-term represents the dissipation of the fluctuation energy due to inelastic particle–particle collision and frictional interactions. The fourth-term represents the exchange of the fluctuation energy due to interphase momentum transport, and the last term representing the dissipation due to interaction with the fluid.

Note that using Eq. 10 the fluctuation kinetic energy Eq. 14 is reduced to the equation of granular temperature of particles used in the original KTGF.[5] We see that the difference of conservation equations between present model and the original KTGF is the equation of solids fluctuating energy. Present model uses the fluctuation kinetic energy e_o to measure the energy associated with the translational and rotational velocities fluctuations of particles in substitute of the granular temperature θ in the original KTGF. Thus, the kinetic theory for rough spheres has the same structure as that for frictionless spheres, i.e., only conservation of mass, translational velocity and fluctuation kinetic energy need to be considered. The modification to the gas–solid two-fluid model is through the introduction of a coefficient of restitution and roughness that incorporate the additional dissipation due to frictional interactions in the rate of dissipation of fluctuation energy. The only equations that need to be modified are the dissipation terms in the fluctuation energy equation and the partial slip boundary condition for the flux of fluctuation kinetic energy to the wall.

Constitutive equations based on the kinetic theory for rough spheres

In accordance with the basic idea of the Chapman-Enskog method, the singlet distribution function is represented as a powers series in[2,32]:

$$f_1 = f_1^{(0)} + f_1^{(1)} + \ldots \tag{15}$$

where $f^{(0)}$ and $f^{(1)}$ are the zero- and first-order function. The above implies the following normalization conditions imposed on f_1[32]

$$\int f_1^{(0)} d^6\Omega_1 = n, \quad \int f_1^{(0)} c_1 d^6\Omega_1 = nu \quad \text{and} \quad \int f_1^{(0)} \omega_1 d^6\Omega_1 = 0 \tag{16}$$

$$\int f_1^{(0)} \left[\frac{1}{2} m|c_1 - u|^2 + \frac{1}{2} I\omega^2\right] d^6\Omega_1 = nme_0 \tag{17}$$

$$\int f_1^{(1)} d^6\Omega_1 = \int f_1^{(1)} c_1 d^6\Omega_1 = \int f_1^{(1)} \left[\frac{1}{2}|c_1 - u|^2 + \frac{1}{2m} I\omega^2\right] d^6\Omega_1 = 0 \tag{18}$$

The distribution function $f^{(0)}$ is independent of spatial gradients of the hydrodynamic properties. It has a form identical to that describing the spatially homogeneous state. From the kinetic theory of gases, the distribution function $f^{(0)}$ may be represented by the Maxwell-Boltzmann distribution function. For flow of rough inelastic particles, it is expressed by Eq. 9. The present $f^{(0)}$ differs slightly from the equilibrium distribution function used for the case of perfectly elastic and perfectly rough spheres by Chapman and Cowling.[2] In that case, energy is conserved and there is equipartition of the mean translational and rotational fluctuation kinetic energies. Here the different degrees of energy dissipation due to particle inelasticity and surface friction are considered. As shown in detail in Chapman and Cowling,[2] the distribution function $f_1^{(1)}$ appearing in Eq. 15 may be represented as a linear combination of the gradients of the hydrodynamic properties n, u, and e_0

$$f_1^{(1)} = -\frac{f_1^{(0)}}{n}\left[A_1^{(1)} \cdot \frac{\partial \ln n}{\partial x} + B_1^{(1)} \cdot \frac{\partial \ln P_c}{\partial x} + C_1^{(1)} \cdot \frac{\partial \ln e_0}{\partial x} + \left(\frac{m}{e_o}\right)^{1/2} (D_1^{(1)} \nabla \cdot u_s + E_1^{(1)} : \nabla^o u_s)\right] \tag{19}$$

where n is the number of particles per unit volume and P_c is the collisional stress tensor of particles. $A_1^{(1)}$, $B_1^{(1)}$, $C_1^{(1)}$, $D_1^{(1)}$, and $E_1^{(1)}$ are functions of the dimensionless velocities $C/e_o^{1/2}$ and $\omega(I/me_o)^{1/2}$. In addition, these coefficient functions depend parametrically upon hydrodynamic properties and upon the

mechanical and geometric properties of granules and the interactions between them. The vector coefficients $A_1^{(1)}$, $B_1^{(1)}$, $C_1^{(1)}$ contribute to the constitutive equation for the kinetic energy flux. The tensor coefficient $E^{(1)}$ contributes to the viscosity, and the scalar $D^{(1)}$ determines the bulk viscosity of particles. In the two classical cases $e = |\beta| = 1$, the $\partial \ln n/\partial x$ and $\partial \ln P_c/\partial x$ terms are absent.[2] The expressions of these coefficient functions are proposed by Goldshtein et al.[39] by means of the Chapman-Enskog method over the entire range of variation of the parameters characterizing the inelasticity and roughness of particles.

From Eq. 15, the expression for the solids pressure tensor p_{ij} is expanded[32]:

$$p_{ij} = p_{ij}^{(0)}(f^{(0)}) + p_{ij}^{(1)}(f^{(0)}) + p_{ij}^{(1)}(f^{(1)}) + \cdots \quad (20)$$

where $p_{ij}{}^{(0)}(f^{(0)})$ in the right-hand sides of Eq. (20) is the zero-order contribution to the stress tensor for the singlet distribution function f. The second term appears due to nonlocal effects arising from the first-order corrections to f, and the third term is due to the local effects arising from the first-order corrections to f. The kinetic part of the pressure tensor $p_{ij}{}^{(0)}(f^{(0)})$ do not depend upon the choice of the collisional model. Similar to the Chapman-Enskog solution,[2] the zero-order solution yields an isotropic stress tensor:

$$p_{ij}^{(0)} = \frac{3}{4}\alpha_t \varepsilon_s \rho_s e_0 \delta_{ij} \quad (21)$$

where δ_{ij} is the unit tensor. To evaluate the first-order contribution to the deviatoric part of the solids pressure tensor, the collisional contribution to the total stress tensor is expressed[30,32]

$$p_{ij}^{(1)} = 3\alpha_t \varepsilon_s^2 \rho_s g_o \eta_1 e_o \delta_{ij} - 1.6\mu_k \varepsilon_s g_o [2\eta_1 + 3\eta_2] S_{ij} - \mu_{dil}\left\{\frac{1 + 1.6[\eta_1(3\eta_1 - 2) + 0.5\eta_2(6\eta_1 - 1 - 2\eta_2 - \frac{2\eta_2\alpha_r}{K\alpha_t})]\varepsilon_s g_o}{g_o[(2 - \eta_1 - \eta_2)(\eta_1 + \eta_2) + \frac{\eta_2^2\alpha_r}{6K\alpha_t}]}\right\} S_{ij} + \frac{192}{5\pi}\eta_2 \mu_{dil} \varepsilon_s^2 g_o \delta_{ij} \times \nabla \times \mathbf{u}_s - \frac{8}{3}\varepsilon_s g_o \sigma \rho_s \sqrt{\frac{e_o}{\pi}}\left[\varepsilon_s \sqrt{\frac{3\alpha_t}{4}} - \frac{\alpha_t \pi}{g_0}\sqrt{\frac{3}{128}}\pi(a_{kt} + 2\varepsilon_s g_o(1+e)a_{ct})\right]\left[\eta_1 \nabla \cdot \mathbf{u}_s \delta_{ij} + \frac{3}{10}(4\eta_1 + 3\eta_2) S_{ij}\right] \quad (22)$$

where S_{ij} is the strain rate tensor. μ_{dil} may be identified as the shear viscosity for perfectly elastic and smooth spheres at dilute concentrations[2]

$$\mu_{dil} = \frac{5\sigma\rho_s}{15}\sqrt{\frac{3\pi\alpha_t e_0}{4}}\frac{(1+K)^2}{6 + 13K} \quad (23)$$

The solid pressure p_s is composed of collisional and kinetic parts, and relates with kinetic energy and concentration of particles

$$p_s = \frac{3}{4}\alpha_t \varepsilon_s \rho_s e_o + \frac{3}{2}\alpha_t \varepsilon_s^2 \rho_s g_o (1+e) e_o \quad (24)$$

$$\alpha_t = \frac{2}{3a}[(a-b) + (a^2 + b^2)^{1/2}],$$
$$a = (1-\beta^2)\frac{1-K}{1+K} - 1 + e^2 \quad \text{and} \quad b = 2K\left(\frac{1+\beta}{1+e}\right)^2 \quad (25)$$

where g_o is the equilibrium radial distribution function at contact, which is independent of particle collisional properties. The first term in Eq. 24 is the kinetic portion, and the second term is the collisional part. We see that the effect of inelasticity of particle collisions is to decrease the collisional transfer pressure part (with respect to the case of elastic collisions) by the factor $(1 + e)$. In addition, both inelasticity and roughness affect solid pressure via the normal restitution coefficient and tangential restitution coefficient. If $\beta = -1.0$, the coefficient α_t is 4/3. While the value of α_t is 2/3 when $\beta = 1.0$ and $e = 1.0$.

The solids shear-stress tensor contains shear and bulk viscosities arising from particle momentum exchange due to collision. The particle phase shear viscosity is given by the sum of a collisional and a kinetic contribution, as shown in the following equation:

$$\mu_s = \mu_{s,kin} + \mu_{s,col} \quad (26)$$

where

$$\mu_{s,kin} = \mu_{dil}\left\{\frac{1 + \frac{8}{5}[\eta_1(3\eta_1 - 2) + 0.5\eta_2(6\eta_1 - 1 - 2\eta_2 - \frac{2\eta_2\alpha_r}{K\alpha_t})]\varepsilon_s g_o}{g_o[(2 - \eta_1 - \eta_2)(\eta_1 + \eta_2) + \frac{\eta_2^2\alpha_r}{6K\alpha_t}]}\right\} \times \left\{1 + \frac{4}{5}[2\eta_1 + 3\eta_2]\varepsilon_s g_o\right\} \quad (27)$$

and

$$\mu_{s,col} = \frac{2}{5}\varepsilon_s g_o \sigma \rho_s \sqrt{\frac{e_o}{\pi}}(4\eta_1 + 3\eta_2)\left[\varepsilon_s\sqrt{\frac{3\alpha_t}{4}} - \sqrt{\frac{3}{128}}\pi\frac{\alpha_t\pi}{g_0}(a_{kt} + 2\varepsilon_s g_o(1+e)a_{ct})\right]$$
$$\alpha_r = \frac{2}{3a}[(a+b) - (a^2+b^2)^{1/2}] \quad (28)$$

The bulk viscosity of particles is

$$\xi_b = \frac{4}{3}\varepsilon_s g_o \sigma \rho_s (1+e)\sqrt{\frac{\theta}{\pi}}\left[\varepsilon_s\sqrt{\frac{3\alpha_t}{4}} - \sqrt{\frac{3}{128}}\pi\frac{\alpha_t\pi}{g_0}(a_{kt} + 2\varepsilon_s g_o(1+e)a_{ct})\right] \quad (29)$$

where the coefficient a_{kt} and a_{ct} are given in Table 1. The spin viscosity is

$$\xi_s = \frac{192}{5\pi}\mu_{dil}\varepsilon_s^2 g_o \frac{K(1+\beta)}{1+K} \quad (30)$$

The energy flux includes the translational energy flux and the rotational energy flux. In accordance with the basic idea of the Chapman-Enskog method, the singlet distribution function is expanded as a powers series expressed by Eq. 15. The expressions for the energy flux q_{ij} is [32]

$$q_{ij} = q_{ij}^{(0)}(f^{(0)}) + q_{ij}^{(1)}(f^{(0)}) + q_{ij}^{(1)}(f^{(1)}) + \cdots \quad (31)$$

where $q_{ij}^{(0)}(f^{(0)})$ is the zero-order contribution to the energy flux for the singlet distribution function f. The second term appears due to nonlocal effects arising from the first-order corrections to the distribution function f, and the third term is due to the local effects arising from the first-order corrections to the distribution function f. The kinetic part of the energy flux $q_{ij}^{(0)}(f^{(0)})$ does not depend upon the choice of the collisional model. Similar to the Chapman-Enskog solution,[2] the zero-order solution yields zero heat diffusion flux

$$q_{ij}^{(0)} = 0 \quad (32)$$

Unlike the classical Chapman-Enskog solution, in the present case of rough inelastic particles, the heat flux is determined not only by the zero order function $f^{(0)}$ but also by $f^{(1)}$. By using arguments of flux homogeneity, we can obtain an equation for energy flux[30,32]

$$q_{ij}^{(1)} = \left\{ \frac{3k_{\mathrm{dil}}}{4g_0\Pi_1}[\alpha_{\mathrm{t}}(\Pi_2+\Pi_4)+\alpha_{\mathrm{r}}(\Pi_3+\Pi_5)] + \frac{9}{5}\varepsilon_{\mathrm{s}}g_0\frac{k_{\mathrm{dil}}}{g_0\Pi_1}(\eta_1+\frac{2}{3}\eta_2)[\alpha_{\mathrm{t}}\Pi_2+\alpha_{\mathrm{r}}\Pi_3] + \frac{3\sqrt{3\alpha_{\mathrm{t}}e_{\mathrm{o}}}}{\sqrt{4\pi}}\alpha_{\mathrm{t}}(\eta_1+\eta_2)\varepsilon_{\mathrm{s}}^2\rho_{\mathrm{s}}g_0\sigma + \frac{2\eta_2}{K}\frac{k_{\mathrm{dil}}}{g_0\Pi_1}\varepsilon_{\mathrm{s}}g_0[\alpha_{\mathrm{t}}\Pi_4+\alpha_{\mathrm{r}}\Pi_5] + \frac{3\eta_2}{K}\varepsilon_{\mathrm{s}}^2\rho_{\mathrm{s}}g_0\sigma\alpha_{\mathrm{r}} \right\} \nabla e_{\mathrm{o}} \quad (33)$$

where k_{dil} may be identified as the thermal conductivity for perfectly elastic and smooth spheres at dilute concentrations

$$k_{\mathrm{dil}} = \frac{25\sigma\rho_{\mathrm{s}}}{128}\sqrt{\frac{3\pi\alpha_{\mathrm{t}}e_0}{4}} \quad (34)$$

where the coefficient Π_i ($i = 1, 5$) is given in Table 1.

The rate of dissipation of fluctuation kinetic energy due to particle collisions and frictional interactions is

$$\gamma_{\mathrm{s}} = -3\varepsilon_{\mathrm{s}}^2\rho_{\mathrm{s}}g_0\alpha_{\mathrm{t}}e_{\mathrm{o}}\frac{3\sqrt{3}}{2\sigma}\sqrt{\frac{\alpha_{\mathrm{t}}e_{\mathrm{o}}}{\pi}}\left[1-e^2+\left(\frac{1-\beta^2}{1+k}\right)\left(K+\frac{\alpha_{\mathrm{r}}}{\alpha_{\mathrm{t}}}\right)\right] + \frac{3\varepsilon_{\mathrm{s}}\rho_{\mathrm{s}}e_{\mathrm{o}}}{4}[C_1\alpha_{\mathrm{t}}+2C_2\alpha_{\mathrm{t}}\varepsilon_{\mathrm{s}}g_{\mathrm{o}}(1+e)]\nabla\cdot u_{\mathrm{s}} \quad (35)$$

The rate of energy dissipation per unit volume resulting from the transfer of gas phase fluctuations to the particle phase fluctuations is predicted using Koch's expression[40] as follows

$$D_{\mathrm{gs}} = \frac{2}{(3\alpha_{\mathrm{t}})^{1.5}}\frac{\sigma\rho_{\mathrm{s}}}{\sqrt{\pi e_{\mathrm{o}}}g_{\mathrm{o}}}\left(\frac{18\mu_{\mathrm{g}}}{\sigma^2\rho_{\mathrm{s}}}\right)^2\left|\mathbf{u}_{\mathrm{g}}-\mathbf{u}_{\mathrm{s}}\right|^2 \quad (36)$$

Numerical solution procedure

Flow behavior of particles in a bubbling fluidized bed is modeled using the kinetic theory for dense, slightly inelastic, slightly rough spheres. The governing equations are given in the previous section. The simulations are carried out with the computational fluid dynamics (CFD) code KTRS-FIX (Kinetic Theory of Rough Spheres-Flow with Interphase eXchanges). This code is based on the modified K-FIX CFD code which previous used in the numerical simulations of fluidized beds.[10,41] The K-FIX code uses a staggered finite difference mesh system.[41,42] In the KTRS-FIX code, the fluctuation kinetic energy e_{o} is used to replace with the granular temperature θ in the K-FIX code. The numerical scheme used in the KTRS-FIX code is the implicit continuous Eulerian approach, and uses donor cell differencing. The conservation of the momentum equations is in explicit form. The continuity equations excluding mass generation are in implicit form. The set of nonlinear equations is linearized using a modified version of the SIMPLE algorithm using the void fraction and gas pressure correction equations. The adaptive time step in the range of 0.00001–0.0005 is used. The time step automatically decreases when the solution is changing more rapidly, and it increases when fast transients subside in order to minimize computation time.

At the inlet, all velocities and volume fractions of gas and particles are specified. The pressure boundary condition is set as atmospheric on the top of the freeboard. At the outlet, the pressure is set to be 1 atm.

At the wall, the gas tangential and normal velocities are set to zero (no slip condition). The normal velocity of particles is also set at zero. The following boundary equations are applied for the tangential velocity and kinetic energy of particles at the wall[43,44]:

$$u_{\mathrm{t,w}} = -\frac{4\mu_{\mathrm{s}}\varepsilon_{\mathrm{s,max}}}{\pi\phi_{\mathrm{sc}}\rho_{\mathrm{s}}\varepsilon_{\mathrm{s}}g_{\mathrm{o}}\sqrt{\alpha_{\mathrm{t}}e_{\mathrm{o}}}}\frac{\partial u_{\mathrm{s,w}}}{\partial n} \quad (37)$$

$$e_{\mathrm{o,w}} = -\frac{3\alpha_t k_s e_{\mathrm{o}}}{4\chi_{\mathrm{w}}}\frac{\partial e_{\mathrm{o,w}}}{\partial n} + \frac{\pi\phi_{\mathrm{sc}}\rho_{\mathrm{s}}\varepsilon_{\mathrm{s}}u_{\mathrm{s}}^2g_{\mathrm{o}}\sqrt{\alpha_t}e_{\mathrm{o}}^{3/2}}{4\varepsilon_{\mathrm{s,max}}\chi_{\mathrm{w}}} \quad (38)$$

where χ_{w} is the energy dissipation due to inelastic collisions between particles and the wall. ϕ_{sc} is the specularity coefficient. The value of the specularity coefficient ranges from zero when collisions between particles and the wall are specular, to unit when incident particles are scattered diffusely. The value of the specularity coefficient of 0.5 suggested by Sinclair and Jackson[45] is used in simulations.

Initially, there are no motions for both the gas and the particles in the bed. The simulations start with the axial gas velocity in the static bed height of $u_{\mathrm{mf}}/\varepsilon_{\mathrm{mf}}$ and u_{mf} in the freeboard region of the bed at $t = 0$, where u_{mf} is the minimum fluidization velocity and $\varepsilon_{\mathrm{mf}}$ is the volume fraction of gas at minimum fluidization. The particle concentration in the freeboard region is set to zero.

Numerical Results and Discussions

Comparison with the experiment of Taghipour et al.

To validate the current numerical model, two-dimensional simulations are conducted in a bubbling fluidized bed. The hydrodynamics of a two-dimensional gas–solid fluidized bed were experimentally studied by Taghipour et al.[38] Experiments were conducted in a 2-D plexiglas column of 1.0 m height, 0.28 m width, and 0.025 m thickness. Spherical glass beads of 250–300 μm diameter and density 2500 kg/m^3 were fluidized with air at ambient conditions. The static bed height was 0.4 m with a solids volume fraction of 0.6. Detail descriptions of the experiments can be found in Taghipour

Table 2. Parameters Used for Taghipour et al.[38] and Simulations

Symbols	Significance	Experiments	Simulations
σ	Particle diameter	250–300 μm	275.0 μm
ρ_s	Solid density	2500 kg/m^3	2500 kg/m^3
μ_g	Gas viscosity	1.789×10^{-5} kg/ms	1.789×10^{-5} kg/ms
u_g	Gas velocity	0.38–0.46 m/s	0.38–0.55 m/s
u_{mf}	Minimum fluidization velocity	0.065 m/s	0.065 m/s
E	Restitution coefficient of particle–particle	No	0.97
β	tangential restitution coefficient	No	−0.5
e_w	Restitution coefficient of particle–wall	No	0.9
ϕ_{sc}	Specularity coefficient	No	0.5
H	Bed height	1.0 m	1.0 m
h_o	Initial bed height	0.4 m	0.4 m
D	Bed diameter	28 mm	28 mm

et al.[38] The parameters of particle–particle and particle–wall interactions used in the present computations are given in Table 2.

Sensitivity of computed bed pressure drop to the spatial grid size is tested. The qualitative impact of the grid on the distribution of simulated bed pressure drop is shown in Figure 1. Three different grids are used, i.e., a coarse grid (20×80), a medium grid (28×100), and a fine grid (42×150). In these trials, it is intended to determine a meshing resolution beyond which the changes in the major parameters are no more significant. Although it is always possible to resolve the local flow parameters further by refining the grid size, the time and/or space averaged operational parameters are expected to remain almost unaffected once a sufficient resolution is reached. Simulated bed pressure drops exhibit the same trends at three different grids, the difference is, however, obvious. The predicted bed pressure drop from coarse grids is larger than that from finer grids. Prediction from both medium grids and finer grids are close to each other. Bubble size is one of the most important parameters in evaluating the performance of bubbling fluidized beds as it controls key characteristics such as bed expansion, solid mixing, gas dispersion, and heat and mass transfer. In this study, a bubble is defined as an area within which the voidage exceeds a threshold value, specified here as $\varepsilon_g = 0.8$.[9,16,46,47] Area of each bubble is measured by a commercial software Image-Pro Plus.[48] Equivalent bubble diameters are calculated from the measured void areas, A, via $D_b = (4A/\pi)^{0.5}$. The variations of averaged bubble size at three different grids are shown in Figure 1. The bubble diameters calculated from the correlation proposed by Darton et al.[49] is also given in. The finer grid tends to predict smaller averaged bubbles. The small differences in bubble diameters between the medium grids and finer grids indicate acceptable grid convergence. In other words, both medium grids and finer grids resolve the motion of bubbles. Therefore, the medium grid sizes are used throughout simulations to reduce the computation times except otherwise stated.

The experimental time-average cross-sectional concentration of particles is compared with the simulation results in Figure 2 at the superficial gas velocity of 0.46 m/s. Both experimental and simulation results show that the concentration of particles is low in the center regime and increase toward the walls. The concentration of particles is highest at the walls. Simulations without the consideration of rotation on the basis of the original KTGF are also given in. Simulated concentration of particles is lower using present model than that by the original KTGF. The trends, however, are the same. Simulated concentrations of particles are in agreement with experimental data.[38]

The boundary condition proposed by Johnson and Jackson[43] is used to simulate flow behavior of particles in the bed. In the Johnson and Jackson boundary condition, the

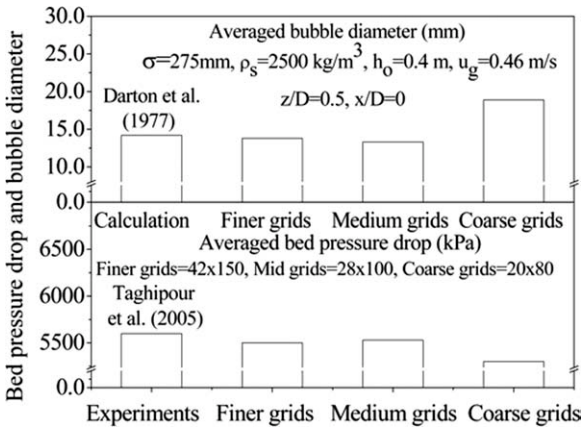

Figure 1. Bed pressure drop and bubble diameters in the bed.

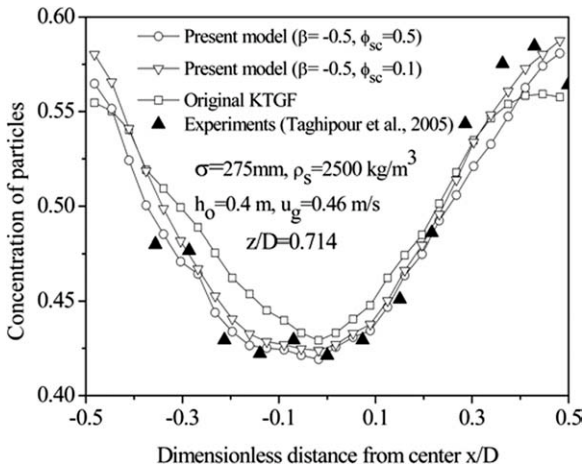

Figure 2. Simulated and measured concentration of particles.

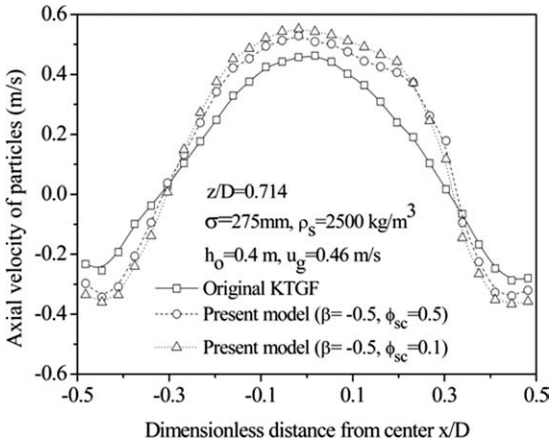

Figure 3. Simulated axial velocity of particles in the bed.

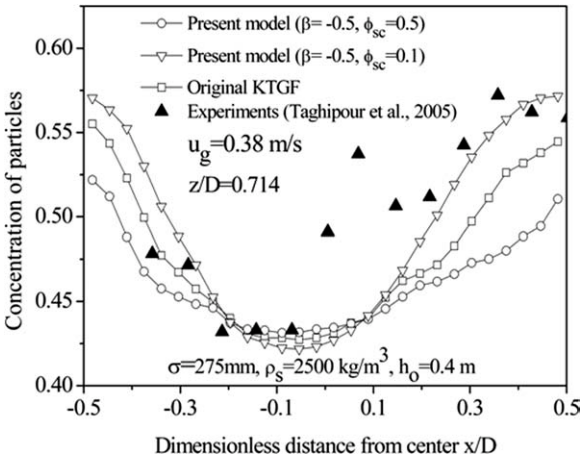

Figure 4. Profile of simulated and measured concentration of particles.

specularity coefficient ϕ_{sc}, characterizing the friction between particles and wall, must be specified. Li et al.[44] investigated the influence of the solid-phase wall boundary condition on flow behavior of particles in numerical simulations of a bubbling fluidized bed. They found that the specularity coefficient impacts on the predicted flow hydrodynamics in the bed. The predicted concentrations of particles for two different specularity coefficients are given in Figure 2. The predicted concentration is high near the walls and low at the center regime of the bed for the specularity coefficient of 0.1. The difference between two specularity coefficients is obvious. However, the trends are the same.

Figure 3 shows the simulated axial velocity of particles at the superficial gas velocity of 0.46 m/s. Both present model and the original KTGF show the axial velocity of particles is high in the center regime and low near the walls. The axial velocity of particles is positive in the center regime, and it is negative near the walls. This means particles flow upward in the center and down-flow near the walls. The circulation of particles is formed in the bed. The simulated axial velocity of particles is larger using present model than that by the original KTGF. Simulated results show that the predicted axial velocity of particles for the specularity coefficient of 0.1 is higher than that at the specularity coefficient of 0.5. The comparison reveals the difference predicted solids circulation patterns between two different specularity coefficients. This suggests that the specularity coefficient may depend on the solid velocity in addition to the particle and wall properties.

The simulated solids concentration profile is compared with experimental data in Figure 4 at the superficial gas velocity of 0.38 m/s. Both simulations and experiments indicate that the concentration of particles is low in the center regime, and increases toward the walls. At $x/D > 0$, the predicted concentration of particles is smaller than that from measurements. Both simulations and measurements give the same trends at $x/D < 0$. From Figures 2 and 4, the increased symmetry of the solid concentration profile is observed for $u_g = 0.46$ m/s compared with $u_g = 0.38$ m/s. Roughly speaking, the simulated concentration of particles is larger from present model than that using the original KTGF. The solid concentrations predicted by present model show reasonable agreement with the experimental data. The simulations between two different specularity coefficients is obvious, when comparing with simulated concentration of particles using the specularity coefficient of 0.5, simulations predict results much more similar to the experimental data with $\phi_{sc} = 0.1$.

The simulated and measured bed expansion ratio h/h_o is compared in Figure 5. Both simulations and experiments demonstrate a consistent increase in bed expansion with superficial gas velocity. Simulated bed expansion ratio using present model is larger than that using the original KTGF. Although the trends between present model and the original KTGF are the same, the difference between models is obvious. When comparing with predictions using the original KTGF, the predicted bed expansion from present model agree well with experiments. Simulations indicate that the predicted bed expansion ratios are seen to be somewhat sensitive to the specularity coefficient. Overall, the bed expansion ratio predicted by the specularity coefficient of 0.1 shows reasonable agreement with the experimental data. Note that in the Johnson and Jackson[43] boundary condition, the specularity coefficient, characterizing the friction between particles and wall, must be specified. The comparison reveals significant

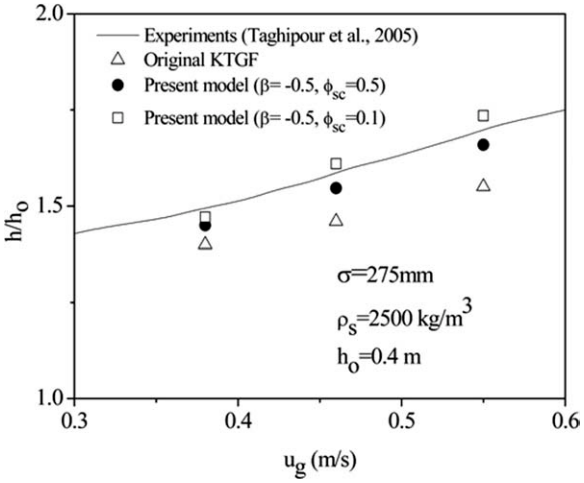

Figure 5. Simulated and measured bed expansion.

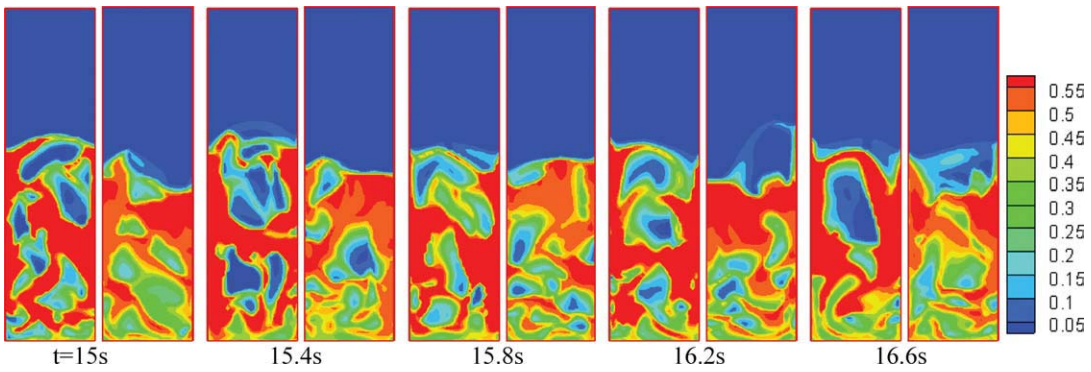

Figure 6. Instantaneous solids concentrations predicted by present model ($\beta = -0.5$) and original KTGF.

[Color figure can be viewed in the online issue, which is available at wileyonlinelibrary.com.]

differences between the specularity coefficients used. Therefore, further investigation is required in future.

Distribution of solids concentration and velocity

A time sequence of solids concentration is shown in Figure 6. Each subfigure has a pair of frames, whereby the left frame shows results from present model and the right frame shows results from the original KTGF (without the friction of particles). Both models give the small bubbles develop near the inlet and travel through the bed, forming larger bubbles by coalescence. Simulations show that present model with $\beta = -0.5$ predicts bigger bubbles and higher gas volume fractions compared with the original KTGF without the friction of particles. The primary reason is that more energy dissipates due to the increase of roughness and particle velocities decrease after impact, leading to a more closely spaced particle ensemble and thus higher porosity. A consequence is that gas–solid interactions exert higher drag forces on particles and cause the particles to move vigorously. Thus, the predictions from present model with the consideration of the friction of particles give a high bubble intensity in the bed.

The instantaneous and time-average local concentrations of particles are analyzed to provide a more detailed look at the bed hydrodynamics. Figure 7 shows an instantaneous local solids concentration fluctuation. The low concentration of particles means a high porosity. The high instantaneous porosity clearly shows the passing of bubbles. A more rapid and irregular development of bubble coalescence is observed, forming very large bubbles. At the bed surface, the high oscillation of concentration of particles is due to the bursting of bubbles. The peaks represented in Figure 7 appear to reflect a bubble frequency.

Figure 8 shows the distribution of concentration of particles at three different bed heights. The profile of time-averaged concentration of particles is not uniform in the bed. The low solids concentration is found in the center regime because the bursting of bubbles is demonstrated with the decreasing concentrations in the center of the bed. Predictions of solids concentration are low at the bed surface since there are larger bubbles is formed. The solid concentrations near the walls are always higher than in other regions of the fluidized bed and close to the maximum packing. Figure 9 shows the profile of axial velocities of gas phase and particles at three different heights. Simulated velocities of gas phase and particles are high in the center regime and low near the walls. The negative value of solid velocity indicates particles flow down near the walls. Thus, the circulation of particles is existed in the bed.

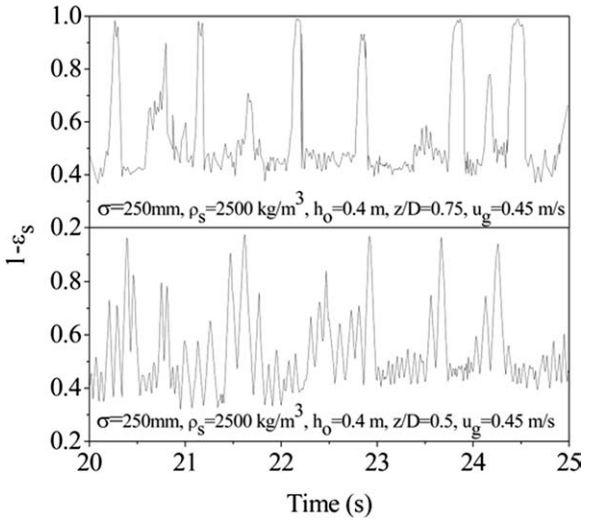

Figure 7. Simulated instantaneous concentrations of particles.

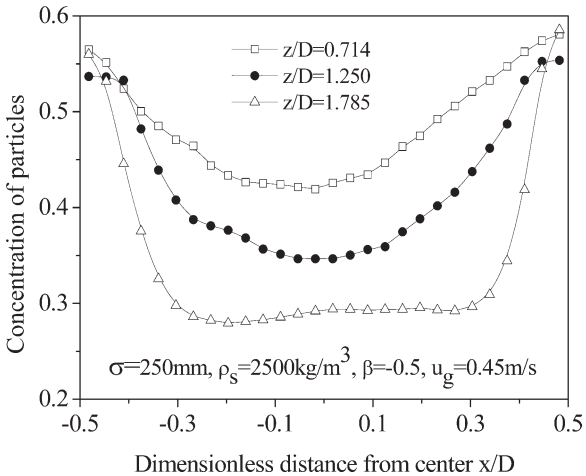

Figure 8. Simulated solids concentration at three positions.

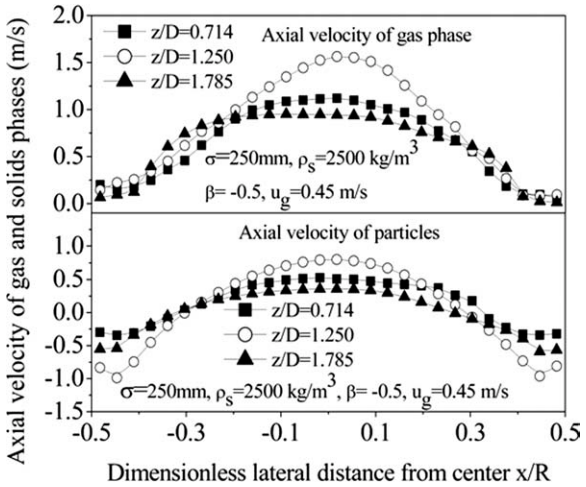

Figure 9. Profile of axial velocity of gas and particles.

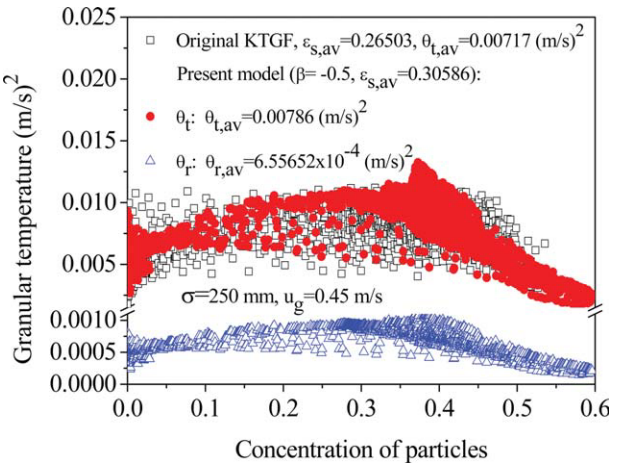

Figure 11. Profile of granular temperature as a function of concentrations.

[Color figure can be viewed in the online issue, which is available at wileyonlinelibrary.com.]

With the continuous introduction of gas from the bottom of the bed, continuously bubbles are formed, which propagate through the fluidized bed. Figure 10 shows the concentration of particles profile predicted by present model and the original KTGF as a function of bed height. These findings are consistent with the simulations by Boemer et al.,[50] who calculated the time-averaged porosity distribution with different approaches of the KTGF. The solid concentrations are always higher in the bed than that at the bed surface.

Figure 11 shows the profile of translational and rotational granular temperature in the bed as a function of concentration of particles. Both the translational granular temperature and the rotational granular temperature increase, reach maximum, and then decrease with the increase of concentration of particles. The mean translational granular temperatures and rotational granular temperature, $\theta_{t,av} = \sum_{i=1}^{N} \theta_{t,i}/N$ and $\theta_{r,av} = \sum_{i=1}^{N} \theta_{r,i}/N$ where N is the total cell number, are 0.00786 $(m/s)^2$ and 0.000656 $(m/s)^2$, respectively. The ratio of the rotational granular temperature to the translational granular temperature is 8.5%. This indicates that the translational granular temperature is on average one-order of magnitude larger than the rotational granular temperature in the bed. The simulated granular temperature from the original KTGF is also given in Figure 11. The predicted granular temperature has the same trends as the translational granular temperature. The computed mean value of granular temperature from the original KTGF is 0.00717 $(m/s)^2$. This value is close to the computed mean translational granular temperature from present model. Recently, the fluctuation velocities and granular temperatures of paired Polyformaldehyde (POM) particles were measured by Chung et al.[51] by means of a particle tracking velocimetry (PTV) technique in a vibrated bed. The study has demonstrated the average rotational granular temperature constitutes $\sim$ 5.4% of the average total granular temperature. It can be expected that the particle rotation in a spherical particulate system should be much greater than that in a nonspherical particulate system. Present simulations and experimental data[51] show that the particle rotation can play a significant role in a vibrated granular bed and fluidized bed.

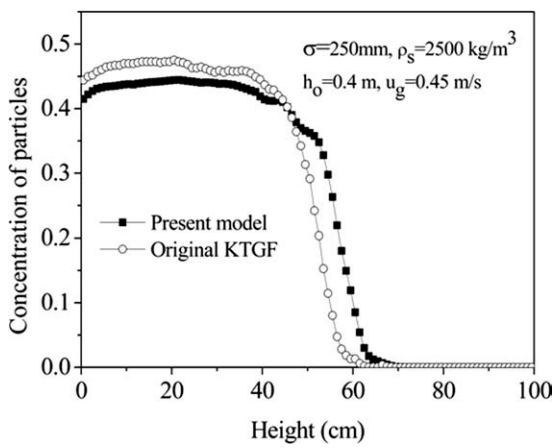

Figure 10. Simulated solids concentrations along bed height.

Effects of roughness coefficients of particles

Particle roughness generally increases the number of degrees of freedom participating in the energy exchange process. Therefore, this property causes retardation of the relaxation process on the one hand, and accelerates energy dissipation on the other. Figure 12 shows the distribution of partition coefficient α_t as a function of roughness and normal restitution coefficient. The partition coefficient increases, reaches a maximum, and then decreases with the increase of roughness. The nonmonotonic character of the β-dependence of partition coefficient α_t may be explained by the following qualitative considerations. The translational kinetic energy loss in a particle collision is independent of β. However, the rotational kinetic energy loss is proportional to $(1 - \beta^2)$, and hence increases with β increasing from -1 to 0.0. In the limiting case of absolutely smooth spheres, $\beta = -1.0$, there is no kinetic energy exchange between the translational and rotational degrees of freedom. Therefore, with increasing β from -1 to 0.0, the rotational kinetic energy loss decreases and the translational kinetic energy loss increases in

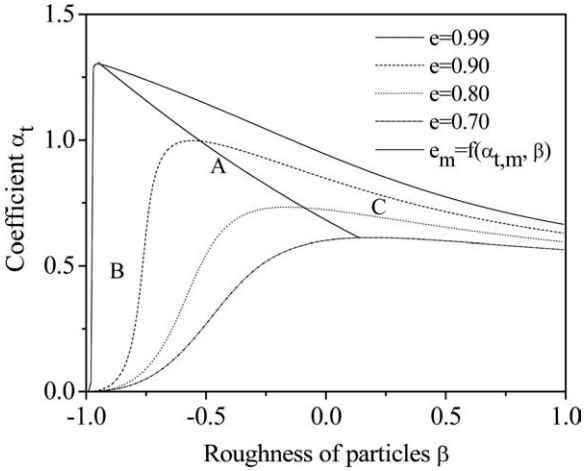

Figure 12. Dependence of partition coefficient upon roughness.

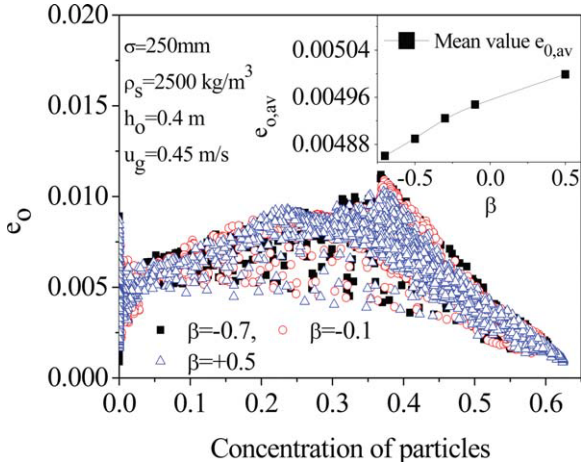

Figure 14. Distribution of kinetic energy of particles as a function of concentrations.

[Color figure can be viewed in the online issue, which is available at wileyonlinelibrary.com.]

accordance with the trend observed in Figure 12. With β further increasing from 0, the rotational kinetic energy loss decreases. However, the kinetic energy exchanged between the rotational and translational modes increases, which leads to a more equal partition of the kinetic energy. These two competitive tendencies result in a β-dependence of coefficient. The effect of increasing particle inelasticity $(1 - e)$ is to increase the kinetic energy. As a result, the granular temperature is redistributed in favor of the rotational modes.

From Figure 12, we see that the partition coefficient α_t reaches a maximum with the change of roughness coefficient at the given coefficient of restitution. The maximum value of β is given in a curve A (β_m). In B regime where $\beta < \beta_m$, the coefficient α_t increases with the decrease of roughness. Although it is reverse in the C regime with $\beta > \beta_m$. For a flow of gas–particle system, the coefficient α_t must decrease with decreasing roughness coefficient. Thus, in further treatment we will consider only the range of parameter $\beta > \beta_m$, where the present hydrodynamic solution exists and possesses physical significance.

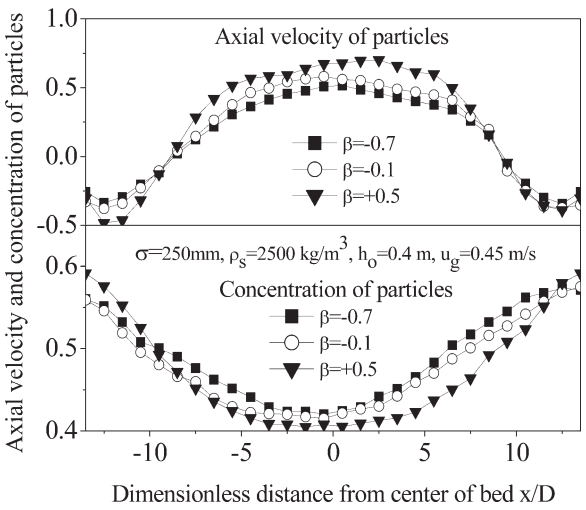

Figure 13. Profile of axial velocity and concentration of particles.

Figure 13 shows a profile of concentration and axial velocity of particles at three different roughness coefficients. Simulations indicate the solid concentration is low in the center regime, and high near the walls. The axial velocity of particles is positive in the center and negative near the walls. The difference is obvious with the change of roughness coefficients. Roughly speaking, the axial velocity of particles is increased and the concentration of particles is decreased with the roughness coefficient from -0.7 to $+0.5$. These means with the change of roughness coefficient from -0.7 to $+0.5$, the fluidized bed height is increased because of the reducing concentration of particles in the bed.

Figure 14 shows the profile of fluctuation kinetic energy of particles as a function of solids concentration. The kinetic energy of random motion contributes from the translational and rotational motion of particles. Simulations show that the fluctuation kinetic energy e_0 increases, reaches maxima, and then decreases with the increase of solids concentrations. For the solids concentration less than 0.1, the mean value of fluctuating kinetic energy $e_{o,av} = \sum_{i=1}^{N} e_{o,i}/N$ is calculated, where N is the total cell number when the concentration of particles in the cell is less than 0.1. We found that in the low solids concentration the averaged fluctuating kinetic energy of particles increase with the increase of roughness. In the dilute flow without particle collisions, the mass, momentum, and energy equations of particles from Eqs. 12–14 are

$$\frac{D\varepsilon_s}{Dt} = -\varepsilon_s \frac{\partial u_s}{\partial x_i} \tag{39}$$

$$\frac{Du_s}{Dt} = -\frac{1}{\varepsilon_s \rho_s}\frac{\partial p}{\partial x_i} \tag{40}$$

$$\frac{3}{2}\varepsilon_s \rho_s \frac{De_o}{Dt} = -\frac{3}{4}\alpha_t \varepsilon_s \rho_s e_o \frac{\partial u_s}{\partial x_i} \tag{41}$$

Combination of the energy conservation equation (Eq. 41) with the conservation of the mass equation (Eq. 39), gives

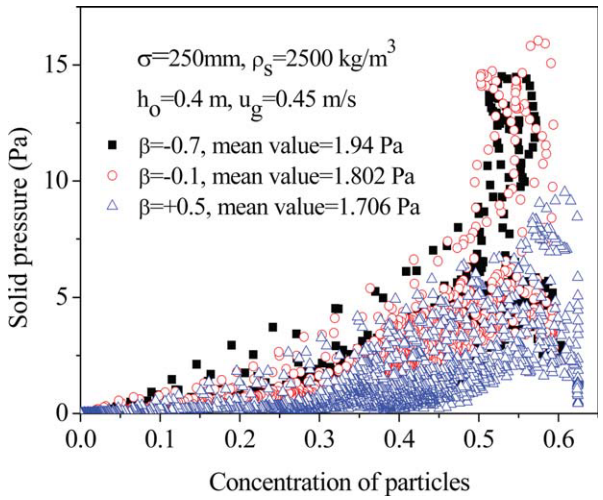

Figure 15. Profile of solid pressure as a function of concentrations.

[Color figure can be viewed in the online issue, which is available at wileyonlinelibrary.com.]

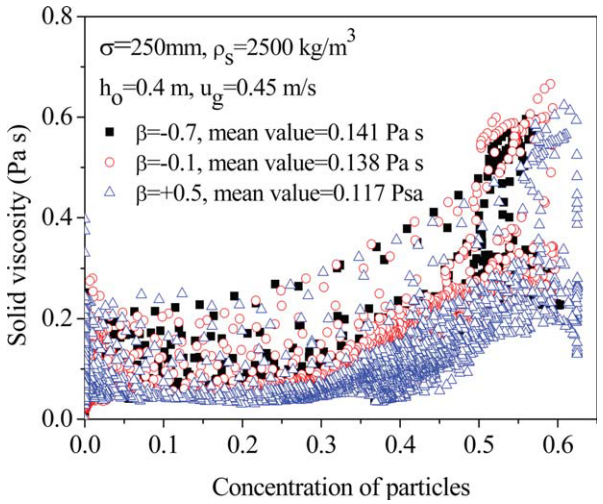

Figure 16. Profile of shear viscosity as a function of concentrations.

[Color figure can be viewed in the online issue, which is available at wileyonlinelibrary.com.]

$$\frac{De_o}{Dt} = -\frac{\alpha_t}{2\varepsilon_s}\frac{D\varepsilon_s}{Dt} \tag{42}$$

This equation shows that the fluctuation kinetic energy e_0 is proportional to the $\alpha_t/2$ power of the solids concentration, as shown below

$$e_o \propto \varepsilon_s^{\alpha_t/2} \tag{43}$$

From Figure 14, we see that the coefficient α_t decreases with the increase of roughness. Therefore, the fluctuation kinetic energy e_o increases with the increase of roughness.

Figure 15 shows the profile of solid pressure as a function of concentration of particles. For three different values of roughness, the solid pressure increases with the increase of solids concentrations. The solids pressure includes the kinetic part and collisional portion. The kinetic part is linearly proportional to solids concentration, while the collisional part is proportional to the square power of solids concentrations. Thus, the solid pressure increases with the increase of concentration of particles.

Figure 16 shows the profile of solid viscosity as a function of solid concentration. Roughly speaking, at the low concentration of particles the solid viscosity is deceased with the increase of solid concentrations. Although at the high concentration of particles, the solid viscosity increases with the increase of solid concentrations. At the very low solid concentrations, the solid viscosity is increased with the decrease of concentration of particles due to the increase of the fluctuation kinetic energy e_0 in Figure 14. The computed mean solid viscosity decreases with the increase of roughness in the bed.

Figure 17 shows the profile of kinetic energy dissipation as a function of concentration of particles. Simulations show that the kinetic energy dissipation increases with the increase of solid concentrations. From Eq. 35, the first term includes the collisional rate of translational kinetic energy interchange and the collisional rate of rotational kinetic energy interchange. It incorporates not only the energy dissipation from inelasticity and surface friction associated with coefficient e and β but also the possible exchange between the translational and rotational kinetic energies. When particles are almost smooth (β close to -1) or almost absolutely rough (β close to 1) the kinetic energy losses due to interparticle friction are small. Accordingly, for these particles all energy losses are associated with the inelasticity of collisions. However, at intermediate values of the roughness (β close to 0) the frictional part of the collisional energy losses is large because of the rotational motion. This is clearly attributed to the kinetic energy losses associated with the translational motion, which losses combine with those arising from particle friction. The second term in Eq. 35 relates to the velocity divergence. This new contribution is not obtained in the original KTGF. The effect of this term is seen to diminish

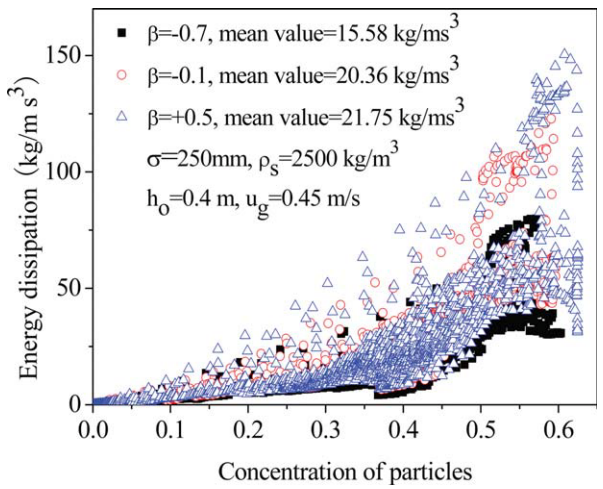

Figure 17. Profile of energy dissipation as a function of concentrations.

[Color figure can be viewed in the online issue, which is available at wileyonlinelibrary.com.]

e_0. This term represents additional energy losses arising from compression of granular media. This term consists of two parts respectively proportional to the kinetic and the collisional solids pressures. For flow of dense particles, the latter part is important for particles undergoing inelastic collisions. With increasing concentration of particles, the intensity of this term increases owing to increasing collisional losses. Therefore, the kinetic energy dissipation increases with the increase of concentration of particles in the bed.

Conclusions

A gas–solid two-fluid model is proposed using a kinetic theory for rapid granular flow of slightly frictional spheres. The kinetic theory for rough spheres is through the introduction of fluctuation kinetic energy associated with fluctuations in both translational velocity and spin. Present approach uses a one equation model to describe the fluctuation kinetic energy of the particle through the introduction of a coefficient of restitution and roughness, considering both dilute and dense cases. Simulations using present model and the original KTGF are performed to study flow behavior of gas and particles in a 2-D bubbling fluidized bed. Results are compared with experimental results in the bubbling fluidized bed. An agreement is achieved by using present model with the consideration of particle rotation where kinetic theory is applicable.

Simulated results show that the computed mean particle viscosity and energy dissipation of particles exhibit nonmonotonic roughness-dependences. Present simulations indicate that the average rotational kinetic energy constitutes ~8.5% of the translational kinetic energy in the bed. Both numerical simulations and theoretical analysis show that at the low solid concentrations the fluctuation kinetic energy of particles increases with the increase of roughness. Preliminary results indicate that particle rotation is an important microscopic physics to be incorporated into the fundamental hydrodynamic model.

Present model is easily generalized to include the dependence of particle roughness and inelasticity upon collisions of particles. As far as the restitution coefficient and roughness are concerned, their values affect the results significantly in numerical simulations. For further model development, the model is validated by comparing its predictions to experiments in bubbling gas-fluidized beds which will be of interest for further investigation. The authors also recognize that the two-dimensional domain reduces the rotation effect. Therefore, particle rotation in a three-dimensional simulation will be addressed in future studies.

Acknowledgments

This work was supported by the Natural Science Foundation of China through Grant No. 51076040.

Notation

a = constant
c = instantaneous velocity of particles (m/s)
A_1 = vector coefficient
B_1 = vector coefficient
C = fluctuation velocity of particles (m/s)
C_1 = vector coefficient
C_d = drag coefficient
D = bed diameter (m)
D_1 = scalar coefficient
D_{gs} = rate of energy dissipation (kg/ms^3)
e = coefficient of normal restitution
e_o = fluctuation kinetic energy (m/s)^2
e_w = wall-particle restitution coefficient
E = kinetic energy of random motion (kg m^2/s^2)
E_1 = tensor coefficient
f = single particle distribution function (s^3/m^6)
$f^{(2)}$ = pair distribution function (s^6/m^{12})
F = external force acting on a particle per mass unit (N/kg)
g = gravitational acceleration (m/s^2)
g_0 = radial distribution function
h_o = height (m)
$\boldsymbol{I}$ = unit tensor
k_s = granular conductivity (kg/ms)
k = particle collision unit vector
K = nondimensional moment of inertia
m = mass of particle (kg)
n = number of particles per unit volume (1/m^3)
p = fluid pressure (Pa)
p_s = solid pressure (Pa)
Re = Reynolds number
t = time (s)
u, v = velocity components (m/s)
u_g = superficial gas velocity (m/s)
u_{mf} = minimum fluidized velocity (m/s)
Yu_s = particle velocity (m/s)
z = bed height (m)

Greek letters

σ = particle diameter (m)
β = tangential restitution coefficient
β_{gs} = fluid-particle drag force coefficient (kg/m^3 s)
γ_c = energy dissipation rate of translational fluctuation (kg/m s^3)
ε_g = voidage or porosity
ε_s = solid volume fraction
$\varepsilon_{s,max}$ = maximum solid packing
θ_t = translational granular temperature (m^2/s^2)
θ_r = rotational granular temperature (m^2/s^2)
μ_g = gas viscosity (kg/ms)
μ_s = particle viscosity (kg/ms)
ξ_b = bulk viscosity (kg/ms)
ξ_s = spin viscosity (kg/ms)
ρ_g = gas density (kg/m^3)
ρ_s = particle density (kg/m^3)
τ = stress tensor (Pa)
χ = source term for collisional rate
δ_{ij} = Kronecker's symbol transported property
ω = particle angular velocity
ϖ = fluctuating angular velocity
α_t = dimensionless coefficient
α_r = dimensionless coefficient
Π = coefficient
ϕ_{sc} = specularity coefficient

Subscripts

g = gas
l = laminar flow
n = normal direction
w = wall

Literature Cited

1. Grace JR, Li T. Complementarity of CFD, experimentation and reactor models for solving challenging fluidization problems. *Particuology*. 2010;8:498–500.
2. Chapman S, Cowling TG. *The Mathematical Theory of Non-Uniform Gases*, 3rd ed. Cambridge: Cambridge University Press, 1970.
3. Grad H. On the kinetic theory of rarefied gases. *Commun Pure Appl Math*. 1949;2:331–407.
4. Jenkins JT, Richman MW. Grad's 13 moment system for a dense gas of inelastic spheres. *Arch Ration Mech Anal*. 1985;87:355–377.

5. Gidaspow D. *Multiphase Flow and Fluidization*. New York: Academic Press, 1994.
6. Ding J, Gidaspow D. A bubbling fluidization model using kinetic theory of granular flow. *AIChE J*. 1990;36:523–538.
7. Peirano E, Delloume V, Johnsson F, Leckner B, Simonin O. Numerical simulation of the fluid dynamics of a freely bubbling fluidized bed: influence of the air supply system. *Powder Technol*. 2002;122: 69–82.
8. Yang N, Wang W, Ge W, Li J. CFD simulation of concurrent-up gas-solid flow in circulating fluidized beds with structure-dependent drag coefficient. *Chem Eng J*. 2003;96:71–80.
9. Gelderbloom SJ, Gidaspow D, Lyczkowski RW. CFD simulations of bubbling/collapsing fluidized beds for three Geldart groups. *AIChE J*. 2003;49:844–858.
10. Huilin L, Gidaspow D. Hydrodynamics of binary fluidization in a riser: CFD simulation using two granular temperatures. *Chem Eng Sci*. 2003;58:3777–3792.
11. Benyahia S, Syamlal M, O'Brien TJ. Evaluation of boundary conditions used to model dilute, turbulent gas/solids flows in a pipe. *Powder Technol*. 2005;156:62–72.
12. Iddir H, Arastoopour H. Modeling of multi-type particle flow using the kinetic theory approach. *AIChE J*. 2005;51:1620–1632.
13. Johansson K, van Wachem BGM, Almstedt AE. Experimental validation of CFD models for fluidized beds: influence of particle stress models, gas phase compressibility and air in flow models. *Chem Eng Sci*. 2006;61:1705–1717.
14. Lindborg H, Lysberg M, Jakobsen HA. Practical validation of the two-fluid model applied to dense gas-solid flows in fluidized beds. *Chem Eng Sci*. 2007;62:5854–5869.
15. Owoyemi O, Mazzei L, Lettieri P. CFD modeling of binary-fluidized suspensions and investigation of role of particle-particle drag on mixing and segregation. *AIChE J*. 2007;53:1924–1940.
16. Leboreiro J, Joseph GG, Hrenya CM, Snider DM, Banerjee SS, Galvin JE. The influence of binary drag laws on simulations of species segregation in gas-fluidized beds. *Powder Technol*. 2008;184:275–290.
17. Almuttahar A, Taghipour F. Computational fluid dynamics of high density circulating fluidized bed riser: study of modeling parameters. *Powder Technol*. 2008;185:11–23.
18. Xie N, Battaglia F, Pannala S. Effects of using two- versus three-dimensional computational modeling of fluidized beds. I. Hydrodynamics. *Powder Technol*. 2008;182:1–13.
19. Cadoret R, Coufort-Saudejaud LC, Pannala S, Syamlal M, Caussat B. Multifluid Eulerian modeling of dense gas-solids fluidized bed hydrodynamics: influence of the dissipation parameters. *Chem Eng Sci*. 2008;63:5540–5551.
20. Igci Y, Andrews AT IV, Sundaresan S, Pannala S, O'Brien T. Filtered two-fluid models for fluidized gas-particle suspensions. *AIChE J*. 2008;54:1431–1448.
21. Li T, Pougatch K, Salcudean M, Grecov D. Numerical simulation of single and multiple gas jets in bubbling fluidized beds. *Chem Eng Sci*. 2009;64:4884–4898.
22. Hosseini SH, Ahmadi G, Rahimi R, Zivdar M, Esfahany MN. CFD studies of solids hold-up distribution and circulation patterns in gas-solid fluidized beds. *Powder Technol*. 2010;200:202–215.
23. Wang J, vanderHoef MA, Kuipers JAM. CFD study of the minimum bubbling velocity of Geldart A particles in gas-fluidized beds. *Chem Eng Sci*. 2010;65:3772–3785.
24. Arastoopour H. Numerical simulation and experimental analysis of gas-solid flow systems: 1999 Fluor-Daniel Plenary lecture. *Powder Technol*. 2001;119:59–67.
25. Gidaspow D, Jung J, Singh RK. Hydrodynamics of fluidization using kinetic theory: an emerging paradigm 2002 Flour-Daniel lecture. *Powder Technol*. 2004;148:123–141.
26. Savage SB, Jeffrey DJ. The stress tensor in a granular flow at high shear rates. *J Fluid Mech*. 1981;110:255–272.
27. Lun CKK, Savage SB, Jeffrey DJ, Chepurniy N. Kinetic theories for granular flow: inelastic particles in curette flow and slightly inelastic particles in a general flow field. *J Fluid Mech*. 1984;140: 223–256.
28. Jenkins JT, Mancini F. Balance laws and constitutive relations for plane flows for a dense, binary mixture of smooth, nearly elastic, circular disks. *J Appl Mech*. 1987;54:27–34.
29. Lun CKK, Savage SB. A simple kinetic theory for granular flow of rough, inelastic, spherical particles. *J Appl Mech*. 1987;54:47–53.
30. Lun CKK. Kinetic theory for granular flow of dense, slightly inelastic, slightly rough spheres. *J Fluid Mech*. 1991;233:539–559.
31. Jenkins JT, Zhang C. Kinetic theory for identical, frictional, nearly elastic spheres. *Phys Fluids*. 2002;14:1228–1235.
32. Goldshtein A, Shapiro M. Mechanics of collisional motion of granular materials, part 1. General hydrodynamic equations. *J Fluid Mech*. 1995;282:75–114.
33. Sun J, Battaglia F. Hydrodynamic modeling of particle rotation for segregation in bubbling gas-fluidized beds. *Chem Eng Sci*. 2006;61:1470–1479.
34. Syamlal M, Rogers W, O'Brien TJ. *MFIX documentation: volume I, theory guide*. *Technical Report* DOE/METC-9411004, NTIS/DE9400087, National Technical Information Service, Springfield, VA, 1993.
35. Shuyan W, Zhiheng S, Huilin L, Long Y, Wentie L, Yonlong D. Numerical predictions of flow behavior and cluster size of particles in riser with particle rotation model and cluster-based approach. *Chem Eng Sci*. 2008;63:4116–4125.
36. Johnson PC, Nott P, Jackson R. Frictional-collisional equations of motion for particles flows and their application to chutes. *J Fluid Mech*. 1990;210:501–535.
37. Shuyan W, Huilin L, Xiang L, Long Y, Jianmin D, Yunhua Z. CFD simulations of bubbling beds of rough spheres. *Chem Eng Sci*. 2008;63:5653–5662.
38. Taghipour F, Ellis N, Wong C. Experimental and computational study of gas-solid fluidized bed hydrodynamics. *Chem Eng Sci*. 2005;60:6857–6867.
39. Goldshtein A, Poturaev VN, Shulyak IA. Structure of the equations of hydrodynamics for a medium consisting of inelastic rough spheres. *Fluid Dyn*. 1990;25:305–313.
40. Koch DL. Kinetic theory for a monodisperse gas-solids suspension. *Phys Fluids A*. 1990;2:1711–1723.
41. Bouillard JX, Lyczkowski RW, Gidaspow D. Porosity distributions in a fluidized bed with an immersed obstacle. *AIChE J*. 1989;35:908–922.
42. Rivard WC, Torrey MD. *K-FIX: A Computer Program for Transient, Two Dimensional, Two Fluid Flow, LA-NUREG-6623*. Los Alamos: Los Alamos National Laboratory, 1977.
43. Johnson PC, Jackson R. Frictional collisional constitutive relations for antigranulocytes materials, with application to plane shearing. *J Fluid Mech*. 1987;176:67–93.
44. Li TW, Grace JR, Bi HT. Study of wall boundary conditions in numerical simulations of bubbling fluidized beds. *Powder Technol*. 2010;203:447–457.
45. Sinclair JL, Jackson R. Gas-particle flow in a vertical pipe with particle-particle interactions. *AIChE J*. 1989;35:1473–1496.
46. Cammarata L, Lettieri P, Micale GDM, Colman D. 2D and 3D CFD simulations of bubbling fluidized beds using Eulerian-Eulerian models. *Inter J Chem Reactor Eng*. 2003;1:48–53.
47. Goldschmidt M, Kuipers JAM, van Swaaij W. Hydrodynamic modeling of dense gas-fluidized beds using the kinetic theory of granular flow: effect of coefficient of restitution on bed dynamics. *Chem Eng Sci*. 2001;56:571–578.
48. Image Pro. *Media Cybernetics, Version 5.1*. MD, USA: Image Pro, 2007.
49. Darton RC, Lanauze RD, Davidson JF, Harrison D. Bubble-growth due to coalescence in fluidized-beds. *Trans Inst Chem Eng*. 1977;55:274–280.
50. Boemer A, Qi H, Renz U. Eulerian simulation of bubble formation at a jet in a two-dimensional fluidized bed. *Inter J Multiphase Flow*. 1997;23:927–944.
51. Chung YC, Hsiau SS, Liao HH, Oi JY. An improved PTV technique to evaluate the velocity field of non-spherical particles. *Powder Technol*. 2010;202:151–161.

Manuscript received Aug. 23, 2010, revision received Dec. 2, 2010, and final revision received Feb. 8, 2011.